Target-Specific Output Patterns Are Predicted by the Distribution of Regular-Spiking and Bursting Pyramidal Neurons in the Subiculum

Yujin Kim and Nelson Spruston*

ABSTRACT: Pyramidal neurons in the subiculum project to a variety of cortical and subcortical areas in the brain to convey information processed in the hippocampus. Previous studies have shown that two groups of subicular pyramidal neurons—regular-spiking and bursting neurons—are distributed in an organized fashion along the proximal–distal axis, with more regular-spiking neurons close to CA1 (proximal) and more bursting neurons close to presubiculum (distal). Anatomically, neurons projecting to some targets are located more proximally along this axis, while others are located more distally. However, the relationship between the firing properties and the targets of subicular pyramidal neurons is not known. To study this relationship, we used in vivo injections of retrogradely transported fluorescent beads into each of nine different regions and conducted whole-cell current-clamp recordings from the bead-containing subicular neurons in acute brain slices. We found that subicular projections to each area were composed of a mixture of regular-spiking and bursting neurons. Neurons projecting to amygdala, lateral entorhinal cortex, nucleus accumbens, and medial/ventral orbitofrontal cortex were located primarily in the proximal subiculum and consisted mostly of regular-spiking neurons (~80%). By contrast, neurons projecting to medial EC, presubiculum, retrosplenial cortex, and ventromedial hypothalamus were located primarily in the distal subiculum and consisted mostly of bursting neurons (~80%). Neurons projecting to a thalamic nucleus were located in the middle portion of subiculum, and their probability of bursting was close to 50%. Thus, the fraction of bursting neurons projecting to each target region was consistent with the known distribution of regular-spiking and bursting neurons along the proximal–distal axis of the subiculum. Variation in the distribution of regular-spiking and bursting neurons suggests that different types of information are conveyed from the subiculum to its various targets. © 2011 Wiley-Liss, Inc.

KEY WORDS: subiculum; bursting; hippocampal formation; information processing

INTRODUCTION

The hippocampal formation is a group of regions that is functionally important in learning and memory. It includes the hippocampus [dentate gyrus (DG), CA3, and CA1], the subicular complex (subiculum, presubiculum, and parasubiculum), and the entorhinal cortex. The subiculum is one of the major output structures from the hippocampal formation. Its primary inputs are from entorhinal cortex, CA1 of hippocampus, and midline thalamic nuclei (Witter, 2006). The subiculum integrates information from these inputs and relays information via its projections to various cortical and subcortical regions (Swanson and Cowan, 1975; Swanson et al., 1981; Donovan and Wyss, 1983; Groenewegen et al., 1987; Witter and Groenewegen, 1990; Witter et al., 1990; Kloosterman et al., 2003).

Previous studies have shown that the subiculum is divided into multiple subregions based on their connectivity. Amaral et al. (1991) and others described a connectional topography along the proximal–distal axis extending from CA3 (proximal) to CA1, subiculum and entorhinal cortex (distal); neurons in proximal subiculum receive inputs from the distal CA1 and lateral entorhinal cortex (LEC), while those in distal subiculum receive inputs from the proximal CA1 and medial entorhinal cortex (MEC; Amaral et al., 1991; Tamamaki and Nojyo, 1995; O'Mara, 2005; Gigg, 2006; Cappaert et al., 2007). In addition to the organized pattern of inputs, output targets are distinct in different portions of subiculum (Meibach and Siegel, 1977; Sørensen, 1980; Witter and Groenewegen, 1990; Canteras and Swanson, 1992; Wyss and Van Groen, 1992; Namura et al., 1994; Verwer et al., 1997; Pitkanen et al., 2000; O'Mara et al., 2001; Witter, 2006). Naber and Witter (1998) described four subregions of subiculum divided by the dorsoventral and the proximodistal axes, each of which serves as the origin of different efferent projections. For example, some subcortical structures, such as lateral septum and nucleus accumbens (NAc), receive inputs from the proximal subiculum, while others, such as ventromedial hypothalamic nucleus (VHN) and amygdala, receive inputs primarily from the ventral subiculum (Witter and Groenewegen, 1990; Canteras and Swanson, 1992; Hirose et al., 1992; Wyss and Van Groen, 1992; Verwer et al., 1997; O'Mara et al., 2001).

The projections from the subiculum to several brain regions could be explained either by a homogenous group of neurons, with each neuron terminating on multiple targets, or by a heterogenous group of neurons, each of which projects to a single region. Naber and Witter (1998) addressed this question by showing that the degree of axonal collateralization of each neuron in the subiculum is very low, indicating that the

Department of Neurobiology and Physiology, Northwestern University, Evanston, Illinois 60208
Grant sponsor: National Institute of Health; Grant number: NS-35180; Grant sponsor: NARSAD Distinguished Investigator Award.
*Correspondence to: Nelson Spruston, Department of Neurobiology and Physiology, Northwestern University, 2205 Tech Drive, Evanston, IL 60208-3520, USA. E-mail: spruston@northwestern.edu
Accepted for publication 6 January 2010
DOI 10.1002/hipo.20931
Published online in Wiley Online Library (wileyonlinelibrary.com).

target specificity of subicular subregion is determined by the distribution of individual neurons with parallel projections. Consistently, other studies using labeling of two different target sites reported only a small fraction of cells (0–30%) projecting to both targets (Swanson et al., 1981; Donovan and Wyss, 1983; Namura et al., 1994).

Pyramidal neurons, which form the primary group of neurons projecting out of the subiculum, can be categorized into at least two groups based on their firing mode: regular-spiking and bursting neurons (Mason, 1993; Mattia et al., 1993; Stewart and Wong, 1993; Taube, 1993; Greene and Totterdell, 1997; Staff et al., 2000; Harris et al., 2001; Cooper et al., 2003; Menendez de la Prida et al., 2003; Jarsky et al., 2008). With brief somatic current injections just above threshold or with antidromic/orthodromic stimulation, regular-spiking neurons fire a single action, whereas bursting neurons produce two or three action potentials at high frequency (Jarsky et al., 2008; Staff et al., 2000; Stewart 1997). In response to long current injections, regular-spiking neurons exhibited spike-frequency adaptation, whereas bursting neurons respond with one or more high-frequency bursts, usually followed by regular spiking (Staff et al., 2000; Harris et al., 2001; Metz et al., 2005; Jarsky et al., 2008). Recent work from our laboratory indicates that regular-spiking and bursting neurons are separate populations of neurons that differ in a number of properties (Graves et al., in revision).

Regular-spiking and bursting neurons are distributed differently in subiculum. Previous studies have shown that the percentage of bursting neurons increases in a gradient along the proximal–distal axis (Staff et al., 2000; Jarsky et al., 2008). Another study reported that bursting neurons are located preferably in the deep layer along the superficial-deep axis (Greene and Totterdell, 1997). Therefore, it appears that bursting and regular-spiking neurons are not spread randomly in the entire subiculum, but distributed in an organized pattern along these axes.

An important question is whether the various targets of subiculum receive input from regular-spiking neurons, bursting neurons, or both. One prediction would be that each subicular target region receives input from different amounts of regular-spiking and bursting neurons, depending on the anatomical location of the cells within subiculum (Fig. 1A). Targets whose inputs originate in proximal subiculum would receive primarily regular-spiking inputs, whereas targets getting inputs from distal subiculum would receive primarily bursting inputs. Alternatively, each target could receive input from only one biophysical population of neurons, regardless of where the projecting neurons are located in subiculum (Fig. 1B). For example, the small fraction of bursting neurons in the proximal subiculum might all project to one particular target region, while the small fraction of regular-spiking neurons in distal subiculum might project to another area. In this scenario, the biophysical properties of the cells projecting to these regions would not be predicted reliably by their anatomical location.

To distinguish between these possibilities, we labeled neurons projecting to nine different targets of the subiculum and determined their anatomical location and biophysical properties. To visualize a group of neurons projecting to a specific region, we injected retrogradely transported, nontoxic fluorescent beads, which enabled us to measure the physiological properties of target-specific neurons (Brown and Hestrin, 2009b). We calculated the percentage of bursting neurons in the entire subiculum as well as in each target group along the proximal–distal axis. By comparing them, we demonstrated that subicular outputs projecting to different regions carried different ratios of bursting information, as determined by the position of the neurons along the proximal–distal axis of the subiculum.

MATERIALS AND METHODS

Surgery

All animal procedures were approved by the Northwestern University Animal Care and Use Committee. Male Wistar rats (Harlan, bodyweight at surgery 240–260 g) were anesthetized with inhalational isoflurane and placed in a stereotaxic frame. About 150–300 nl of a dilute suspension of fluorescently labeled latex microspheres (red or green RetroBeads, Lumafluor) was loaded into a glass micropipette and injected into the target area at 75 nl/min. Buprenorphine (0.05 mg kg^{-1}) was administered to reduce postsurgical pain. In the case of double injections, two target areas were injected with different colors of beads sequentially. The color of the beads did not affect the labeling efficiency. The stereotaxic coordinates [modified from Paxinos and Watson (2007)] are in millimeters: amygdala (AP −2.3, ML +5.0, and DV −7.8); LEC (AP −5.3, ML +6.8, and DV −8.0); NAc (AP +1.7, ML +1.5, and DV −8.0); medial and ventral orbitofrontal cortex (OfC; AP +4.3, ML +0.4, and DV −5.0); interanteromedial thalamic nucleus (ITN; AP −1.8, ML +0.3, and DV −7.5); MEC (AP −7.6, ML +4.5, and DV −4.5); presubiculum (AP −7.0, ML +4.0, and DV −5.0); retrosplenial cortex (RsC; AP −5.5, ML +1.0, and DV −2.0); and VHN (AP −2.3, ML +0.5, and DV −9.0). The rats were dissected after 2–5 days of recovery. To confirm the injection sites, the brain was sectioned either horizontally (Fig. 2A) or coronally (Fig. 2B).

Histology: Tissue Fixation

To visualize the overall distribution of bead-containing neurons in subiculum (Figs. 3 and 4; $n = 15$), animals were anesthetized with inhalational isoflurane and transcardially perfused with 0.1 M phosphate buffer (PB), pH 7.4, followed by 4% paraformaldehyde. The brain was removed and postfixed in 4% paraformaldehyde overnight at 4°C. The brain was then cryoprotected with 30% sucrose in 0.1 M PB until it sank. Horizontal sections (50 μm) made with freezing microtome (Leica Microsystems) were mounted on a glass slide and coversliped.

For Nissl staining in Figure 3A, the slices on a glass slide were air-dried for 3 days and immersed in 70 and 95% ethanol and xylene for 4 min each. The slices were then immersed back through 95% and 70% ethanol for 2 min each. They

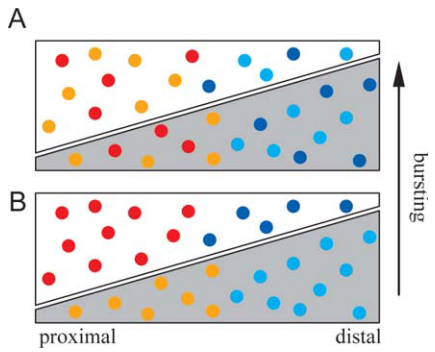

FIGURE 1. Schematic illustration of possible distributions of subicular neurons projecting to different targets. The gray area shows that the propensity to burst increases in a gradient along the proximal–distal axis. The colored circles indicate neurons projecting to four different targets. A: Each target region receives inputs from a different ratio of regular-spiking and bursting neurons. B: Each target region receives inputs from only regular-spiking or bursting neurons. [Color figure can be viewed in the online issue, which is available at wileyonlinelibrary.com.]

were stained for 5 min in filtered cresyl violet solution. After a brief rinse in distilled water, the slices were dehydrated in 70 and 95% ethanol for 1 min each and in xylene for 10 min.

Slice Preparation and Patch-Clamp Recording

Animals were decapitated under deep isoflurane anesthesia, and the brain was transferred in an ice-cold dissection solution containing in mM: 110 choline Cl, 0.2 NaCl 2.5 KCl, 1.25 NaH_2PO_4, 25 $NaHCO_3$, 15 dextrose, 2.4 Na pyruvate, 1.3 ascorbic acid, 0.5 $CaCl_2$, and 3 $MgCl_2$ (pH 7.4, oxygenated with 95% CO_2 and 5% O_2). Three hundred-micrometer-thick horizontal slices were sectioned from the injected hemisphere using a vibrating tissue slicer (Vibratome 3000) and were transferred to a suspended mesh within a chamber filled with artificial cerebrospinal fluid (ACSF) containing in mM: 119 NaCl, 2.5 KCl, 1.25 NaH_2PO_4, 25 $NaHCO_3$, 25 dextrose, 2 $CaCl_2$, and 1 $MgCl_2$ (pH 7.4, oxygenated with 95% CO_2 and 5% O_2) at 35°C. After 30 min of incubation, the chamber was cooled down to room temperature. Most experiments were done with slices acquired between −8.0 mm and −4.0 mm from the bregma in depth, which included ventral and intermediate hippocampus.

All recordings were done with the slices submerged in the recording chamber on the microscope (Axioskop2 FS, N.A. 0.8 Zeiss) stage and constantly perfused with oxygenated ACSF at 33–35°C. Whole-cell current-clamp recordings were performed from the retrogradely labeled neurons identified under epifluorescent illumination using patch pipettes with resistances of

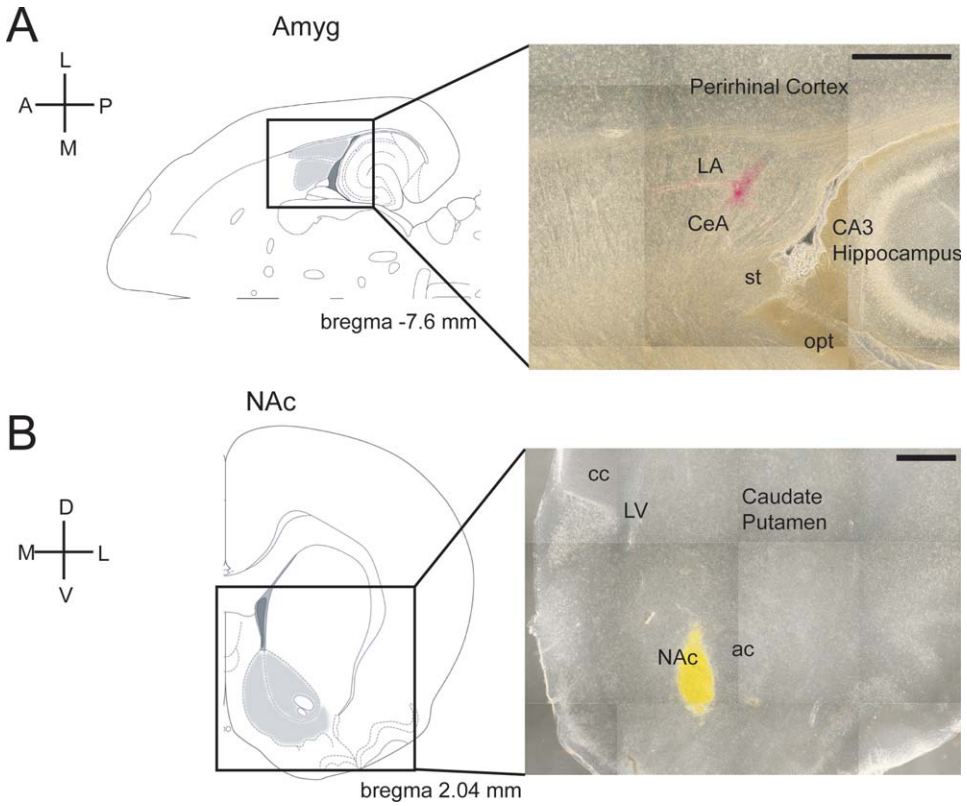

FIGURE 2. Examples of the injection sites. A: Horizontal section from an amygdala-injected animal with red beads and corresponding atlas illustration (Paxinos and Watson, 2007). B: Coronal section from a nucleus accumbens-injected animal with green beads and corresponding atlas illustration (Paxinos and Watson, 2007). Gray areas on the atlas illustrations show the targeted regions. ac, anterior commissure; cc, corpus callosum; CeA, central amygdala; LA, lateral amygdala; LV, lateral ventricle; opt, optic tract; st, stria terminalis; Scale bars, 0.5 mm. [Color figure can be viewed in the online issue, which is available at wileyonlinelibrary.com.]

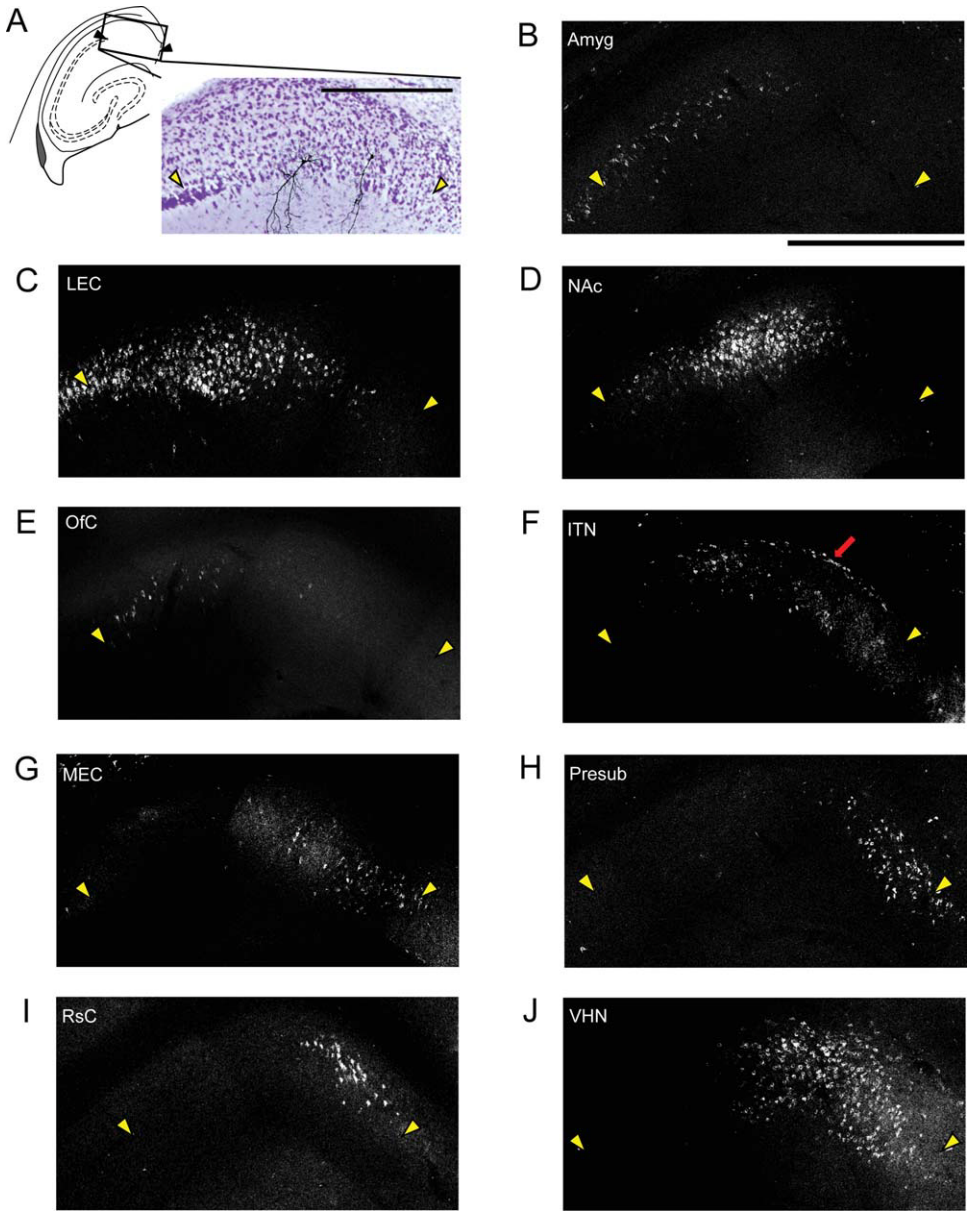

FIGURE 3. Bead-containing neurons in subiculum for each injection site. A: Diagram of the hippocampus and bright-field image of the subiculum in Nissl-stained section. The neurons in black represent the morphology of the neurons studied. B–J: Beads were injected to Amyg (B), LEC (C), NAc (D), OfC (E), ITN (F), MEC (G), Presub (H), RsC (I), and VHN (J). The subicular neurons labeled by each injection are shown in micrographs from an epifluorescence microscope. Red arrow in F shows ITN-projecting neurons in the deep layer. Not all the images are from the same dorsal–ventral axis. Scale bars: 0.5 mm.

3–5 MΩ when filled with an intracellular solution containing (in mM): 115 K-gluconate, 20 KCl, 10 Na_2-phosphocreatine, 10 HEPES, 4 Mg-ATP, 0.3 Na-GTP, and 0.1% biocytin. Recordings were obtained using a Dagan BVC-700 amplifier, low-pass filtered at 3 kHz, and collected using Igor Pro software (Wavemetrics). We identified pyramidal neurons based on firing properties and sag in response to a 1-s current step and subsequently verified pyramidal neuron morphology following biocytin staining. In the rare cases (<1 in 100 neurons) where recordings did not indicate pyramidal cell properties (i.e. continuous spiking >50 Hz during current injections), the data were not collected. The average number of cells recorded was 7.2 ± 0.6 per animal from a total of 58 animals.

The firing pattern of a neuron was determined by the profile of action potentials at threshold. To measure the biophysical properties of action potentials, ten 2-ms-long current steps were injected at 2 Hz. Threshold-level current injections were defined as producing spiking on half of the 10 current injections. In bursting cells, the initial current injection resulted in a burst but many of the later current injections produced only a single spike. In regular spiking cells, all spikes were single spikes (i.e., not bursts). In both cell types, we also increased

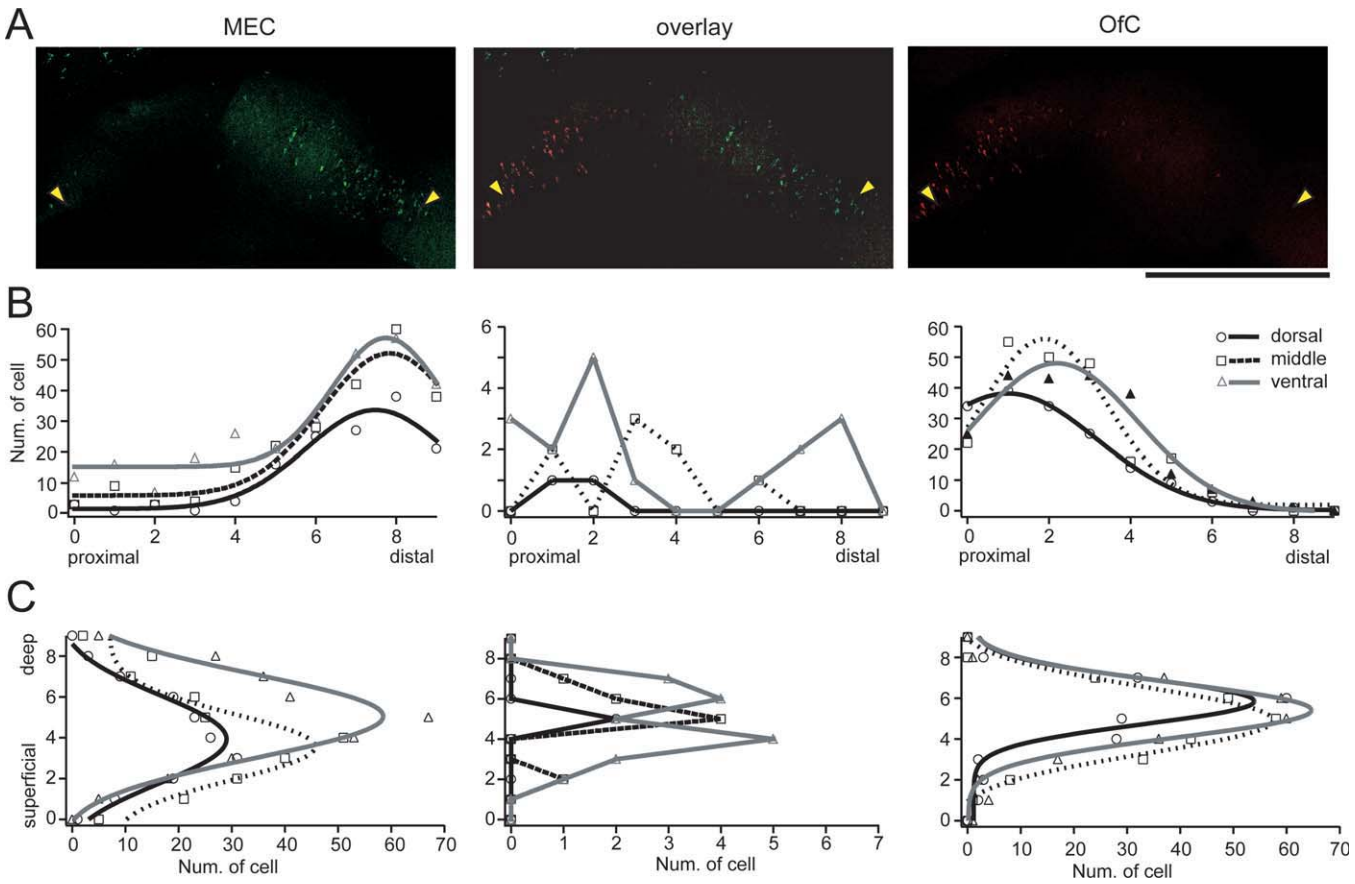

FIGURE 4. An example of the distribution of subicular neurons from a double injection. An animal was injected with green beads in MEC and red beads in OFC. A: Subicular neurons projecting to MEC (left), OFC (right), and both (overlay, middle) in the same horizontal slices are shown. Note the limited overlap between cells labeled by the two injections. Scale bar: 0.5 mm. B, C: The number of neurons projecting to each target in dorsal (circle), middle (square), and ventral (triangle) slices were counted and plotted as a function of distance along the proximal–distal axis (B) or the superficial-deep axis (C). Left, right panels: lines indicate Gaussian fits of the data for dorsal (solid black), middle (dotted black), and ventral (solid gray) slices. No significant differences were found in the distribution of neurons along the dorsal–ventral axis. Middle panels: double-labeled neurons were few in number and randomly distributed in the subiculum. Note the 10-fold smaller scale in the middle panels of B and C.

the current injection to a level that produced bursts on half of the 10 trials, thus allowing us to compare the excitability of the two cell types in response to stronger current injections.

Biocytin Staining

To visualize the cells recorded, slices were fixed in 4% paraformaldehyde and perforated in blocking solution including 3% normal goat serum, 0.5% Triton X-100, and 0.01% sodium azide in 0.1 M PB for 1 h. TRITC-conjugated streptavidin (016–020–084, Jackson Immunoresearch Laboratory) in blocking solution was then applied to the slices for 2 h on a rocker at room temperature. After thorough rinsing with 0.1 M PB, the slices were mounted on the slide glass in Vectashield mounting medium (H-1000, Vector laboratory).

Imaging and Cell Identification

Flourescent images were collected by an Olympus FSX-BSW epifluorescence microscope (Olympus) or a Leica DM IRE2 attached to a confocal laser scanning system (SP2, Leica) equipped with multiple lasers. The laser lines used to excite green and red beads were 488 (Ar laser) and 543 nm (Green HeNe laser), respectively. To visualize bead-containing neurons clearly, *Z*-stacks of five 1-μm-thick optical sections were collapsed.

To determine the location of neurons in subiculum, we drew an arc—an extension of the pyramidal cell layer of CA1 (*stratum pyramidale*)—from the border of CA1-subiculum to the border of subiculum–presubiculum. With one spot on the granule cell layer of the DG at an equal distance to each end of the arc, the subiculum was divided into 64 bins (8 × 8). The size of each bin is one-eighth of the arc length along the proximal–distal axis and one-16th of the radius of the arc along the superficial-deep axis. The border between CA1 and the subiculum is not completely clear, and so we considered a small number of recordings obtained from cells in the most distal CA1 to be in proximal subiculum (position 0 on the proximal–distal axis), thus extending the grid to include a total of

72 bins (Fig. 3A). All data acquisition and analysis were performed using IGOR Pro software (Wavemetrics)

Data Analysis

Input resistance was calculated from steady-state subthreshold voltage changes in response to 600-ms current steps ranging from −200 to 200 pA. The sag ratio was defined as the ratio of the steady-state voltage change to the maximal voltage change (Jarsky et al., 2008). Spike threshold was determined by the maximum of the second derivative of V_m by time, which corresponded to the inflection point at the beginning of an action potential. Amplitude was defined as the difference between the resting membrane potential and the peak voltage, and full width at half maximum amplitude was the time difference at half-maximal spike amplitude. Rise and decay of the action potential was defined as the rate of voltage change in the 10–90% of amplitude in the rise or decay phase. Normalized ΔI was the current amount to evoke multiple spikes normalized to the current amount at threshold.

The physiological properties of nine different targeting groups were compared using one-way analysis of variance (ANOVA). When only two groups were compared (for example, bursting and regular-spiking neurons), two-tailed Student's *t*-test was used. To examine the distribution of neurons along the proximal–distal axis, we considered positions 0–2 as proximal subiculum and positions 6–8 as distal subiculum. On the superficial-deep axis, positions 1–3 were regarded as superficial subiculum and positions 6–8 as deep subiculum.

The relationship between the fraction of bursting and distribution in subiculum along the two axes (Fig. 7C) was evaluated by the correlation coefficient (Pearson's r). The relative probability of bursting neurons along the proximal–distal axis in each target group was compared to those in the full set of neurons using Monte Carlo hypothesis testing based upon resampling the full data. The probability of bursting ($p_i[A]$) for a number of neurons ($n_i[A]$) at location i and targeting a particular area (A) was compared to the probability of bursting at location i in the full data set (p_i). By resampling $n_i[A]$ neurons from the full data set, we obtained an estimate of the probability of bursting at location i (s_i) independent of whether or not a particular area was targeted. The null hypothesis ($H0$) is that the probability of bursting in location i does not depend upon targeting area A (i.e., $p_i[A]$ is not different from s_i). To produce a statistic that allows such a comparison across all locations (i), the sum-of-squares difference (D) between s_i and $p_i[A]$ was calculated as:

$$D = \mathrm{sum}_i[(s_i - p_i[A])^2]/k$$

where i is the position in which cells targeting area A were found and k the number of positions in which cells targeting area A were found.

For example, if cells targeting area A were found in positions 0, 1, and 2, the D value would be

$$D = [(s_1 - p_1[A])^2 + (s_2 - p_2[A])^2 + (s_3 - p_3[A])^2]/3$$

By repeating this process m times (10,000 times in this experiment), we calculated the empirical distribution of D_m under H0 to determine the probability that the actual observation D_A,

$$D_A = [(p_1 - p_1[A])^2 + (p_2 - p_2[A])^2 + (p_3 - p_3[A])^2]/3$$

where D value from area A would be drawn from the empirical distribution. This P-value was estimated as

$$P \text{ value of observation} \cong Pr(D_m \geq D_A) \cong (\#\text{ of } D_m \geq D_A)/m$$

RESULTS

Distribution of Subicular Neurons Projecting to Different Targets

To determine the anatomical distribution of subicular neurons based on their projection, we injected retrogradely transported fluorescent beads into one of the nine target areas: amygdala (Amyg), LEC, NAc, medial and ventral OfC, ITN, MEC, presubiculum (Presub), RsC, and VHN. In horizontal sections, the neurons were identified by epifluorescence in their cell body (Fig. 3). Consistent with previous studies, neurons were not randomly distributed in subiculum. Rather, the neurons were grouped by their projection and, in most cases, occupied either the proximal or distal part of subiculum (Figs. 3B–J). Neurons projecting to Amyg, LEC, OfC, and NAc were distributed in the proximal subiculum while those projecting to MEC, Presub, RsC, and VHN were positioned in the distal half. Interestingly, many of ITN-projecting neurons (but not all) were found in the deep layer of subiculum (Fig. 3F).

Characteristics of Subicular Efferent Projections: Double-Labeling Study

Earlier anatomical studies using retrogradely transported dyes have shown that subicular pyramidal neurons have very few axon collaterals. In studies using injections of labels into multiple target sites, a small fraction of cells (0–30%) was double labeled (Swanson et al., 1981; Donovan and Wyss, 1983; Namura et al., 1994; Naber and Witter, 1998). To confirm the previous findings with the fluorescent beads used here, we injected red and green fluorescent beads to label six pairs of regions. An example from one pair of injections is shown in Figure 4A. In agreement with previous studies (Swanson et al., 1981; Donovan and Wyss, 1983), labeled neurons from two injections sites were not colocalized. The number of double-labeled cells was low, with values ranging from 0% for Amyg/RsC and LEC/RsC to 5.6% for Amyg/OfC (Table 1). One example, a MEC/OfC injection pair is shown in Figure 4. The distribution of the neurons projecting to each area was consistent with the previous observations (Figs.

TABLE 1.

Summary of Labeled Cells by Injection Area from Double-Labeling Study

Area 1	Area 2	Area 1 only (n_1)	Area 2 only (n_2)	Double-labeled (n_d)	Double-labeled $n_d/(n_1 + n_2 - n_d) \times 100$ (%)
Amyg	OfC	233	258	26	5.6
Amyg	RsC	65	254	0	0
ITN	RsC	421	106	2	0.4
LEC	RsC	254	62	0	0
LEC	VHN	503	163	4	0.6
MEC	OfC	651	590	27	2.2

3E,G); that is, MEC-projecting neurons were mostly found in the distal subiculum while OfC-projecting neurons were mostly found in the proximal subiculum, with no overlap between the two populations (Figs. 4A,B).

To pool the distribution information obtained from slices at different dorsoventral positions, we divided the subiculum of each slice into nine by eight bins and scaled the position of each neuron (see Materials and Methods section). Using this approach, we found that the distribution pattern of MEC-projecting neurons as well as OfC-projecting neurons was conserved in dorsal, middle, and ventral sections (Figs. 4B,C). This result was consistently observed in the other groups of target-sharing neurons, except amygdala-targeting neurons, which were found exclusively in ventral subiculum (data not shown).

Biophysical Properties of Subicular Pyramidal Neurons

To measure the physiological properties of neurons, we performed whole-cell patch clamp recordings from 406 randomly selected bead-containing subicular pyramidal neurons projecting to one of the nine target areas (Table 2). To examine the intrinsic properties of neurons, 600-μs-long hyperpolarizing and depolarizing current steps were injected until action potentials were evoked (Fig. 5A). Consistent with previous studies, we observed two different types of firing patterns (Mason, 1993; Mattia et al., 1993; Stewart and Wong, 1993; Taube, 1993; Greene and Totterdell, 1997; Staff et al., 2000; Harris et al., 2001; Menendez de la Prida et al., 2003; Jarsky et al., 2008; Graves et al., in revision). In response to current injections just above threshold, one group of neurons showed an initial burst of action potentials (2–3 spikes at >100 Hz) followed by either additional bursts or regularly spaced action potentials, defined as bursting neurons (Fig. 5A, top). The second group responded to the same stimulus with regularly spaced action potentials, defined as regular-spiking neurons (Fig. 5A, bottom). In this study, our recordings included 218 regular-spiking neurons and 188 bursting neurons.

We examined the biophysical properties in a subset of neurons by measuring three subthreshold properties ($n = 375$) and five suprathreshold properties ($n = 259$), as summarized in Table 2. The input resistance of regular-spiking neurons was significantly higher than that of bursting neurons, and the sag ratio was larger in regular-spiking neurons than in bursting neurons. There was no significant difference in resting membrane potential of the two groups of cells.

The firing properties were measured from a spike in response to 5-ms long current injections just above threshold, which evoked action potentials in half of the trials (Fig. 5B, left). All the five measures indicated that action potentials at threshold in the two classes of neurons were different. Spikes in bursting neurons were narrower and had a more hyperpolarized threshold and larger amplitude compared to spikes evoked in regular-spiking neurons (Table 2). The spikes also rose more steeply and more rapidly in bursting neurons.

To examine how neurons responded to stronger depolarization, we increased current injection to evoke two spikes on half of the 10 trials delivered at 2 Hz (Fig. 5B, right; see Materials and Methods section). Some neurons failed to fire two spikes by the maximal current amount (2 nA; 11 regular-spiking and 4 bursting neurons). Among the neurons where the criterion could be reached ($n = 259$), we found that it required significantly more depolarizing current in regular-spiking neurons than in bursting neurons (Table 2). Although using this stimulus the first spikes in the burst from each cell type were similar, the following spikes differed in regular-spiking and bursting neurons. Specifically, the second spikes were broader, smaller in amplitude, and slower to rise and decay in regular-spiking neurons (Table 2 and Fig. 5B). We subdivided neurons according to their projections and compared the resting and active membrane properties, but could not find any significant differences in any of the measured parameters (one-way ANOVA; Table 2).

The Relationship Between Projection, Output Mode, and Position in the Subiculum

As shown in Figure 4, neurons projecting to most regions were not found along the entire proximal–distal axis of the subiculum, but only in a portion of it. Here, we analyzed the distribution of target-labeled and physiologically characterized neurons in the subiculum (Fig. 6A; $n = 240$ from 33 animals). The fraction of bursting neurons in those neurons was 55%,

TABLE 2.

Subthreshold- and Suprathreshold Membrane Properties of Subicular Pyramidal Neurons

	B	RS	Amyg	LEC	OfC	NAc	ITN	MEC	RsC	VHN	Presub
% of bursting (*n*)	(188)	(218)	15.2 (33)	15.7 (51)	18.0 (50)	25.0 (64)	57.4 (68)	82.1 (28)	75.0 (43)	76.1 (46)	91.3 (23)
Subthreshold											
R_{in} (MΩ)	41.6 ± 0.9	60.8** ± 2.0	62.9 ± 4.4	52.3 ± 3.9	55.5 ± 4.5	52.6 ± 3.1	53.6 ± 3.2	47.5 ± 2.8	44.7 ± 2.3	45.9 ± 3.3	47.4 ± 5.5
Sag ratio	0.98 ± 0.07	1.56** ± 0.12	1.33 ± 0.16	1.72 ± 0.20	1.55 ± 0.13	1.67 ± 0.29	1.58 ± 0.15	1.55 ± 0.14	1.38 ± 0.09	1.24 ± 0.09	1.74 ± 0.14
V_{rest} (mV)	−69.7 ± 0.3	−68.4 ± 0.3	−69.5 ± 0.9	−68.0 ± 0.6	−68.4 ± 0.7	−67.6 ± 0.5	−69.5 ± 0.5	−70.7 ± 0.6	−69.3 ± 0.8	−70.3 ± 0.5	−68.7 ± 0.8
N	174	201	21	45	49	57	44	34	30	46	22
Suprathreshold, at threshold											
Threshold (mV)	−52.2 ± 0.3	−50.5** ± 0.4	−50.6 ± 0.8	−49.0 ± 1.5	−52.0 ± 0.5	−48.8 ± 0.9	−51.3 ± 0.5	−51.7 ± 0.5	−53.0 ± 0.4	−52.7 ± 0.5	−52.2 ± 1.2
Amplitude (mV)	93.0 ± 0.5	91.0** ± 0.7	91.6 ± 1.0	90.5 ± 2.6	94.5 ± 1.2	85.1 ± 2.6	90.6 ± 0.6	92.8 ± 0.9	94.2 ± 1.1	93.2 ± 0.8	93.0 ± 1.2
Full width at half maximum amplitude (ms)	0.66 ± 0.01	0.72** ± 0.01	0.83 ± 0.03	0.74 ± 0.02	0.77 ± 0.02	0.67 ± 0.01	0.64 ± 0.01	0.72 ± 0.02	0.57 ± 0.01	0.62 ± 0.01	0.68 ± 0.02
Rise (*d*V/*dt*)	367 ± 3	341** ± 4	331 ± 7	345 ± 16	349 ± 8	327 ± 13	359 ± 4	356 ± 6	379 ± 8	374 ± 6	354 ± 8
Decay (*d*V/*dt*)	−133 ± 2	−118** ± 2	−97 ± 3	−109 ± 4	−109 ± 4	−118 ± 3	−129 ± 2	−121 ± 3	−169 ± 4	−141 ± 3	−138 ± 5
N	147	112	21	10	31	15	60	46	17	40	19
Suprathreshold, multiple spikes											
Threshold first spike	−53.0 ± 0.3	−53.2 ± 0.5	−53.4 ± 0.9	−52.6 ± 2.4	−54.5 ± 0.9	−49.9 ± 1.1	−52.8 ± 0.5	−53.5 ± 0.6	−54.5 ± 0.7	−53.2 ± 0.6	−52.2 ± 1.2
Second spike	−46.5 ± 0.4	−42.7 ± 0.5	−42.4 ± 1.0	−42.7 ± 2.9	−44.9 ± 1.0	−42.0 ± 1.3	−46.3 ± 0.5	−46.4 ± 0.6	−50.0 ± 0.8	−47.7 ± 0.6	−46.1 ± 1.4
Amplitude first spike	89.3 ± 0.5	88.3 ± 0.7	89.2 ± 0.9	87.9 ± 2.9	91.8 ± 1.8	82.6 ± 2.2	87.5 ± 0.6	89.2 ± 0.8	90.8 ± 1.1	88.9 ± 0.9	92.0 ± 1.1
Second spike	72.7 ± 0.7	68.0** ± 1.1	60.7 ± 2.2	62.2 ± 5.2	67.4 ± 2.4	64.5 ± 2.4	71.8 ± 1.1	71.8 ± 1.4	77.1 ± 1.8	74.4 ± 1.4	73.9 ± 2.0
FWHMA[a] first spike	0.66 ± 0.01	0.71** ± 0.01	0.81 ± 0.02	0.75 ± 0.02	0.76 ± 0.02	0.68 ± 0.02	0.64 ± 0.01	0.71 ± 0.02	0.58 ± 0.01	0.62 ± 0.01	0.68 ± 0.01
Second spike	0.92 ± 0.01	1.12** ± 0.03	1.43 ± 0.11	1.32 ± 0.11	1.16 ± 0.04	1.03 ± 0.03	0.92 ± 0.02	1.02 ± 0.04	0.77 ± 0.01	0.85 ± 0.02	0.94 ± 0.03
Rise first spike	351 ± 3	331** ± 4	328 ± 6	333 ± 17	338 ± 9	315 ± 12	345 ± 4	342 ± 6	362 ± 8	355 ± 6	342 ± 8
Second spike	232 ± 5	176** ± 6	124 ± 10	142 ± 21	172 ± 11	173 ± 12	220 ± 7	215 ± 10	265 ± 10	242 ± 10	221 ± 13
Decay first spike	−129 ± 2	−115** ± 2	−94 ± 3	−103 ± 4	−106 ± 4	−111 ± 3	−124 ± 2	−118 ± 3	−165 ± 4	−134 ± 3	−136 ± 5
Second spike	−69.4 ± 1.0	−65.4* ± 1.6	−54.0 ± 3.1	−55.0 ± 3.7	−57.8 ± 2.1	−66.3 ± 2.9	−70.5 ± 1.3	−64.6 ± 1.8	−82.3 ± 2.3	−76.3 ± 1.7	−69.0 ± 3.6
ISI (ms)	3.14 ± 0.55	3.94** ± 0.05	4.39 ± 0.11	4.20 ± 0.15	3.98 ± 0.13	3.74 ± 0.11	3.69 ± 0.09	1.96 ± 1.78	3.39 ± 0.06	3.76 ± 0.16	3.83 ± 0.15
Norm I (%)	184 ± 4	219** ± 4	245 ± 12	214 ± 10	219 ± 10	196 ± 8	187 ± 6	196 ± 9	194 ± 5	176 ± 5	211 ± 9
n	143	101	18	8	27	15	57	44	17	39	19

*$P < 0.05$,
**$P < 0.001$; compared to B (*t*-test).
[a]Full width at half maximum amplitude.

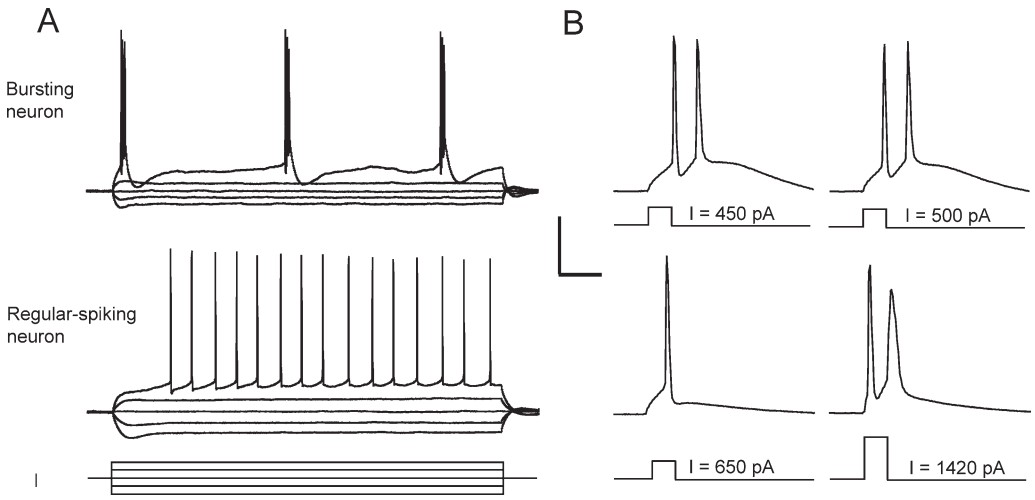

FIGURE 5. Voltage recordings from bursting (top) and regular-spiking (bottom) neurons. A: Responses to 600-ms long current steps from −200 to 200 pA with 100 pA interval. B: 5-ms long brief current steps were injected to evoke spikes at threshold (left) and multiple spikes (right). Scale bar: x = 100 ms for A, x = 10 ms for B; y = 40 mV for (A) and (B).

which was not significantly different from that of the entire group ($P > 0.6$, Fisher's exact test).

As in the fluorscence data without recordings (Fig. 4), we observed a nonuniform distribution of recorded neurons along the proximal–distal axis (Fig. 6B). Neurons projecting to Amyg, LEC, OfC, or NAc were located preferentially in the proximal two-thirds of subiculum, and none of neurons in the distal one-third of subiculum projected to these four regions. On the other hand, neurons terminating in MEC, Presub, or RsC were found in the distal two-thirds of subiculum, and none of the proximal neurons projected to these regions. Neurons projecting to ITN or VHN were distributed along the entire proximal–distal axis. Among the recorded neurons, there was no target specificity along the superficial-deep axis (Fig. 6C).

We also analyzed the relationship between the firing mode of the recorded neurons and their distribution in subiculum. In agreement with previous studies (Staff et al., 2000; Jarsky et al., 2008), there was a correlation between the fraction of bursting neurons and the position in the subiculum, with the proportion of bursting increasing in a gradient along the proximal–distal axis (correlation coefficient $r = 0.95$; Figs. 6B, 7A). This result indicated that 11% of neurons in proximal subiculum were bursting neurons, whereas 91% of neurons in distal subiculum were bursting neurons. By contrast, the correlation coefficient along the superficial-deep axis was very low ($r = 0.09$) (Figs. 6C, 7A). However, all the most superficial neurons were in distal subiculum (arrow in Fig. 7B); when these neurons were excluded, the correlation along the superficial-deep axis became significant ($r = 0.94$). Jarsky et al. (2008) argued that the bursting tendency found along the superficial-deep axis is a sampling artifact, influenced by the strong increase in bursting along the proximal–distal axis. In keeping with this interpretation, we found no correlation along the superficial-deep axis if neurons were divided into separate groups of proximal and distal neurons ($r = 0.23$ for proximal and $r = 0.50$ for distal). Therefore, we find no strong evidence for a correlation of bursting along the superficial-deep axis.

As different brain areas receive inputs from neurons in different parts of subiculum, we examined whether there was a relationship between firing properties and targeting. The percentages of bursting neurons projecting to Amyg, LEC, OfC, and NAc were below 25%, while the percentages of bursting neurons projecting to Presub, MEC, VHN, and RsC were greater than 75% (Table 2 and Fig. 7C). When the relationship between the percentage of bursting and the distribution of subicular neurons of each efferent projection was plotted, the individual plots had a similar tendency toward a greater proportion of bursting in more distal positions (Figs. 7D,E). We therefore analyzed the data to determine if the degree of bursting in each group was consistent with the position of those neurons along the proximal–distal axis, as would be predicted from the tendency in the full data set. To do so, we devised a Monte Carlo-based statistical analysis to determine the likelihood that an observed distribution (for a particular target region) would be sampled from the full data set (see Materials and Methods). In most groups, this probability was greater than 5%, indicating that the distribution of bursting in each group was not significantly different from that of the full data set (Table 3). For NAc-projecting neurons, there were even fewer bursting neurons than expected from their relatively proximal location within the subiculum. For OfC-projecting neurons, there were even more bursting neurons than predicted from their relatively distal location.

DISCUSSION

A full understanding of neural circuits requires not only an understanding of the connections between morphologically

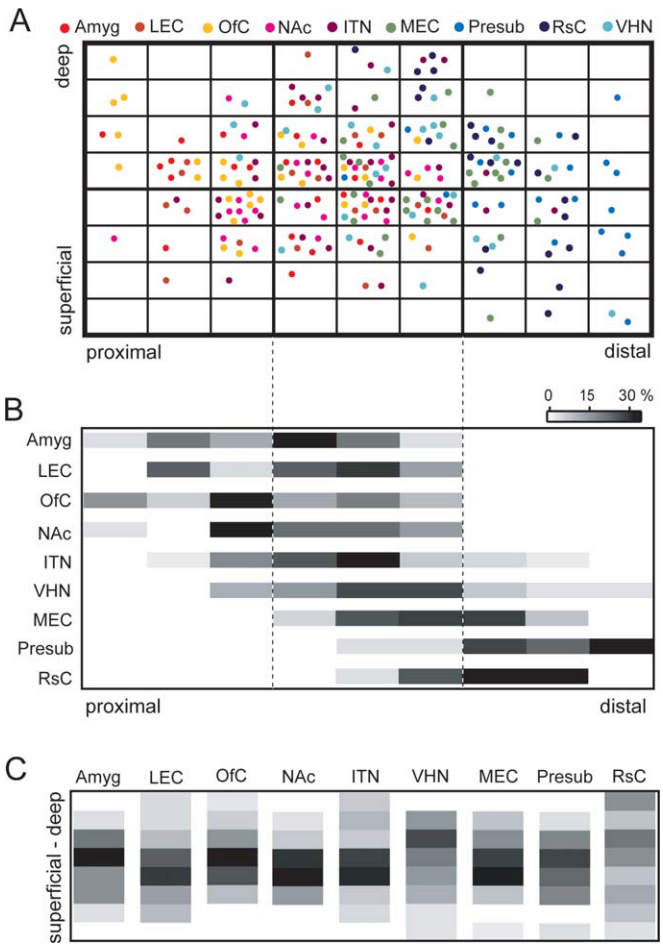

FIGURE 6. Distribution of labeled pyramidal neurons recorded in the subiculum. A: Scatter plot of neurons along the proximal-distal and superficial-deep axes (n = 240). Individual neurons were indicated by different colors based on labeling by injections into the indicated target sites. For interactive version, see http://groups.nbp.northwestern.edu/spruston/figures/hippocampus_2011_6a. B: Percentage of neurons in each position along the proximal-distal axis. Dotted lines divide subiculum on this axis into three subregions: proximal, middle, and distal. C: Percentage of neurons in each position along the superficial-deep axis. [Color figure can be viewed in the online issue, which is available at wileyonlinelibrary.com.]

defined classes of neurons (e.g., pyramidal neurons) but also the further elaboration of connections between physiologically identified neurons (Brown and Hestrin, 2009a). The subiculum is a prime example of this need because of the coexistence of regular-spiking and bursting pyramidal neurons as well as the large number of structures targeted by individual neurons. Here, we addressed the important question of whether particular targets of the subiculum are selectively innervated by regular-spiking or bursting neurons. We find that most targets receive input from both classes of cells, with the fraction of each predictable from the known distribution of these neurons along the proximal–distal axis of the subiculum.

Anatomical Distribution of Subicular Neurons Based on Efferent Targets

Numerous anatomical studies have shown that the extrinsic connections from subiculum are organized along the proximal-distal, superficial-deep, and dorsal–ventral axis (Swanson and Cowan, 1975; Swanson et al., 1981; Donovan and Wyss, 1983; Groenewegen et al., 1987; Witter and Groenewegen, 1990; Witter et al., 1990; Kloosterman et al., 2003). In agreement with previous studies (Witter et al., 1990; Naber and Witter, 1998; Witter, 2006), proximal and distal subregions in subiculum projected to different groups of brain regions. We found that some of the neurons projecting to ITN were located in the deepest layer (Fig. 2). One explanation of this result is that neurons in different superficial-deep layers show target-preferences as previously shown (Ishizuka, 2001). However, neurons projecting to the other eight areas did not show laminar selectivity along the superficial-deep axis, and even ITN-projecting neurons were not restricted to the deep layer. Thus, it appeared that the distributed organization of subicular efferent projections is stronger along the proximal–distal axis than along the superficial-deep axis.

Within each subregion, neurons terminating in different targets were not segregated by their efferent projections, but occupied overlapping portions of the subiculum (Fig. 6A; see also the interactive version, referenced in the figure legend). This is consistent with the observation reported by Swanson et al. (1981) that neurons targeting EC and septum were indistinguishable in their position.

Individual subicular neurons showed an apparently low level of collateralization (Table 1 and Fig. 4), as only 0–5.6% of neurons targeted two regions in six pairs of double injections. We observed the highest percentage of double-labeled neurons by injecting two targets that receive inputs from the same (proximal) subregion of subiculum (5.6% in the Amyg/OfC pair). The percentages of double-labeled neurons in the other pairs were even lower (0–2.2%; Table 1). If we assume that Amyg-projecting neurons also project to all three other proximal-originated targets with the probability of 5.6% and to four distal-originated targets with 2.2%, we could estimate the level of collateralization as high as 25.6%. This is still in the range (0–30%) that has been previously reported (Swanson et al., 1981; Donovan and Wyss, 1983; Namura et al., 1994; Naber and Witter, 1998).

Biophysical Properties of Subicular Pyramidal Neurons

Based on their firing properties, there are two distinct populations of pyramidal neurons in subiculum: regular-spiking and bursting neurons. Along with the different output patterns, the two groups of neurons appeared to show slightly different membrane properties (Greene and Totterdell, 1997; Jarsky et al., 2008). Moreover, they exhibit different patterns of bursting in response to repeated current injections, and their intrinsic excitability is regulated by different mechanisms

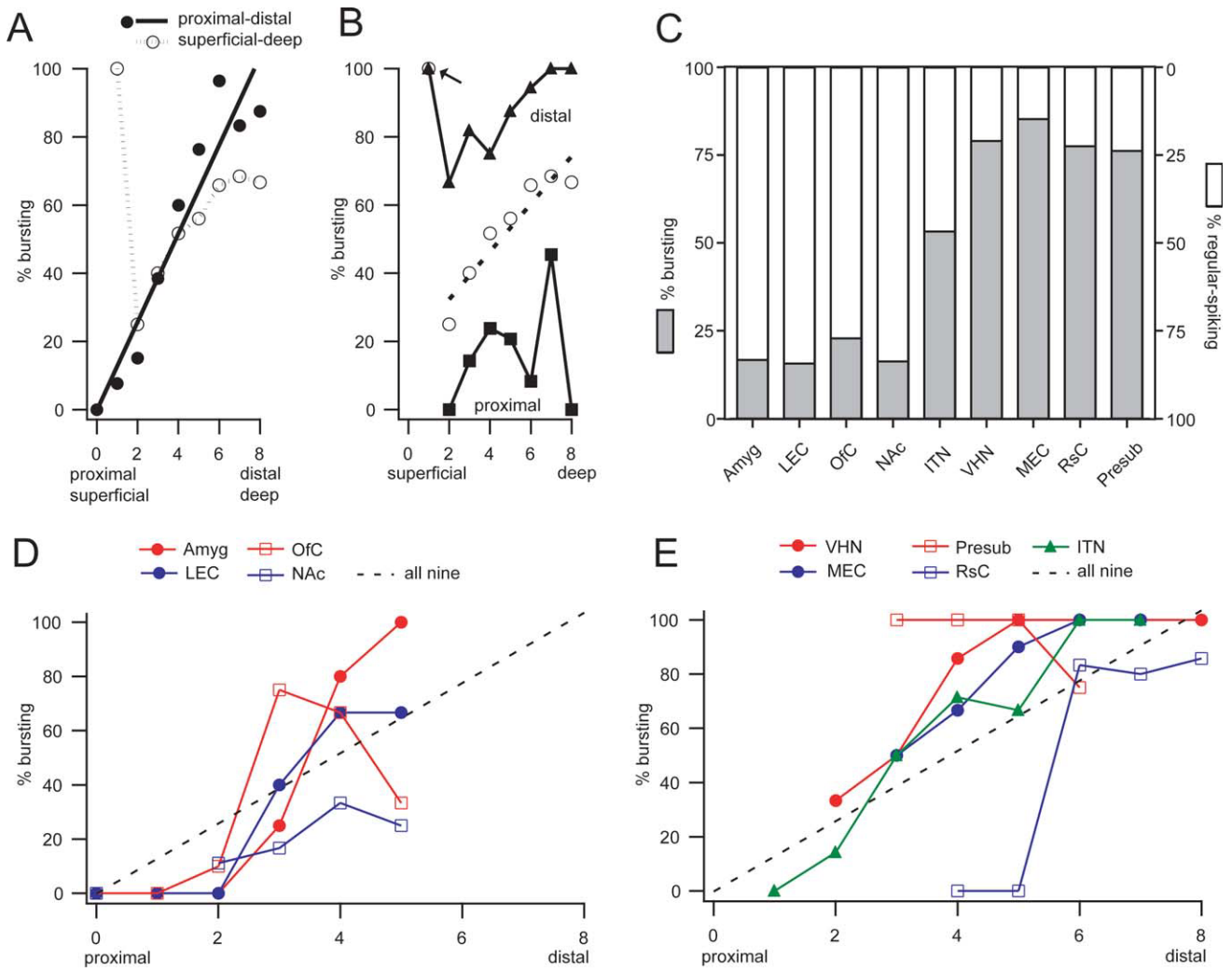

FIGURE 7. Distribution of bursting neurons and their projections. A: Percentage of bursting neurons along the proximal–distal axis (filled circles) and the superficial-deep axis (open circles). The proportion of bursting neurons increases in a gradient toward distal subiculum. The solid line is a linear fit of the distribution along the proximal–distal axis ($r = 0.95$). No significant relationship was found along the superficial-deep axis ($r = 0.09$). B: The correlation between the percentage of bursting and position in the superficial-deep axis was significant (open circles) when the most superficial neurons were excluded (arrow; $r = 0.94$); however, this correlation was not observed when proximal or distal neurons were considered separately ($r = 0.23$ for proximal neurons, filled squares; $r = 0.50$ for distal neurons, filled triangles). C: Percentage of bursting and regular-spiking neurons in each target region. D,E: Percentage of bursting neurons in each target group shown as a function of location along the proximal–distal axis. Dotted line represents the linear correlation found by combining data from all nine groups of neurons (same as the solid line in panel A).

(Graves et al., in revision). Our results showed that the two types of neurons were different not only in firing mode, but also in most subthreshold as well as suprathreshold properties. We found that the electrophysiological differences of regular-spiking and bursting neurons were more significant than reported before; for example, our results suggest that the regular-spiking and bursting neurons differ in their spike threshold, amplitude, and rate of rise. In contrast, no significant differences in these measures were found in our previous study (Staff et al., 2000), perhaps owing to the short current injections

TABLE 3.

The Significance of the Relationship Between the Bursting Along the Proximal-Distal Axis in Each Target Group Compared to the Full Data Set

	Amyg	LEC	OfC	NAc	ITN	MEC	RsC	VHN	Presub
P-value	0.563	0.667	0.002	<0.001	0.923	0.596	0.915	0.065	0.131

used to evoke spikes in the current study, compared to long current injections in the previous study. Indeed, when we injected currents large enough to evoke bursting in regular-spiking cells, the threshold and amplitude of the initial spike were not significantly different in regular-spiking and bursting neurons. This indicates that the disparity in initial spike properties between the two groups is the most noticeable with inputs just above threshold. With the larger current injections, however, the differences in active properties were greater when the second spike in a burst was compared between cell types. The second spike was slower, smaller, and broader, and the interspike interval was significantly longer in regular-spiking neurons than in bursting neurons, perhaps at least partly due to the larger current injection required to evoke bursting in regular-spiking cells. These observations support the conclusion that regular-spiking neurons are a separate class of neurons from bursting neurons [see also Graves et al. (in revision)].

Earlier studies reported that bursting neurons were found more frequently in distal subiculum (Staff et al., 2000; Jarsky et al., 2008; see also Harris et al., 2001). Jarsky et al. (2008) calculated the proportion of bursting neurons as 33% in the proximal subiculum and 60% in the distal subiculum. Here, we confirmed that the fraction of bursting increased in a gradient along the proximal–distal axis. Our data showed a steeper relationship between bursting and anatomical position (11% proximal third and 91% distal third), possibly because the neurons that we chose were limited to those projecting to one of the nine regions.

We could not detect consistent differences in biophysical properties when population of neurons projecting to different target areas were compared. One of the reasons that the membrane properties were not target-specifically different might be that all the groups were composed of a combination of regular-spiking and bursting neurons. However, with our experimental design consisting of a comparison of nine groups, a very large number of cells would have been required to detect significant differences using ANOVA.

The Relationship Between Biophysical Properties and Anatomical Distribution of Subicular Neurons in the Context of Efferent Projection

By analyzing the physiological and anatomical position of subicular neurons, we addressed the hypothesis that subicular output neurons to individual target structures are composed of both regular-spiking and bursting neurons, with the ratio being determined by the anatomical location of the cells within the subiculum. Under this hypothesis, we would observe a strong relationship between the properties of neurons and their position within the subiculum, regardless of their efferent target. Alternatively, each subicular target structure would exclusively receive either bursting or regular-spiking inputs. In this case, there would be a stronger relationship between the firing property of neurons and their efferent target.

We found that the biophysical properties of the neurons projecting to each target were predicted by their anatomical location, which supports our hypothesis. None of the target regions receives inputs exclusively from regular-spiking or bursting neurons [in contrast with a previous report; Stewart (1997)]. Rather, each receives input from a different mixture of bursting and regular spiking information. Amyg, LEC, OfC, and NAc receive inputs from the proximal subicular neurons, which are primarily regular-spiking neurons, while MEC, Presub, RsC, and VHN receive inputs from neurons located in the distal subiculum, which are primarily bursting neurons. When the fraction of bursting neurons in each target was plotted as a function of the location in the subiculum, it followed the positive relationship between the percentage of bursting neurons in the entire subicular neurons and their distribution. In other words, each target region receives a different fraction of regular-spiking and bursting inputs based on the position of the projecting neurons and the distribution of regular-spiking and bursting neurons within the subiculum.

Firing Properties of Subicular Neurons and Intrinsic/Extrinsic Connections From Hippocampus

The connections between CA3 and CA1 and between CA1 and subiculum are not random, but rather have a spatial organization, which can be regarded as at least two distinct streams of information (Ishizuka et al., 1990; Amaral et al., 1991; Gigg, 2006). In one stream, proximal CA3 projects to distal CA1, which in turn projects to proximal subiculum. In another stream, distal CA3 projects to proximal CA1, which in turn projects to distal subiculum. Given that the distribution of bursting neurons increases along this axis in CA3 (Masukawa et al., 1982) and in subiculum (Jarsky et al., 2008), the nature of the information conveyed in these two streams is likely to be different. The percentage of bursting neurons is relatively low in the entire CA1, and so the amount of bursting in each output stream is determined primarily by the bursting properties and anatomical location of neurons in subiculum (Jarsky et al., 2008) and CA3 (Masukawa et al., 1982). The present study indicates that the two streams of information are conserved in output patterns from the subiculum to various target regions (Fig. 8). For example, RsC receives input from distal subiculum (high bursting), which in turn originates in distal CA3 (high bursting). In contrast, amygdala receives input from proximal subiculum (low bursting), which originates in proximal CA3 (low bursting). Thus, regions targeted by neurons in distal subiculum carry more information in the form of bursting than regions targeted by proximal subiculum.

Functional Implications of Different Burst-Firing in Pyramidal Neurons of Subiculum

The different propensities to burst in hippocampal regions observed in vitro appears to be an accurate indication of firing properties in vivo. For example, CA3 neurons in vivo exhibit more bursting than CA1 neurons (Sneider et al., 2006). This difference is likely related to the different responses of the neurons in vitro in that CA3 pyramidal neurons fire an initial high-frequency burst and CA1 pyramidal neurons show tonic

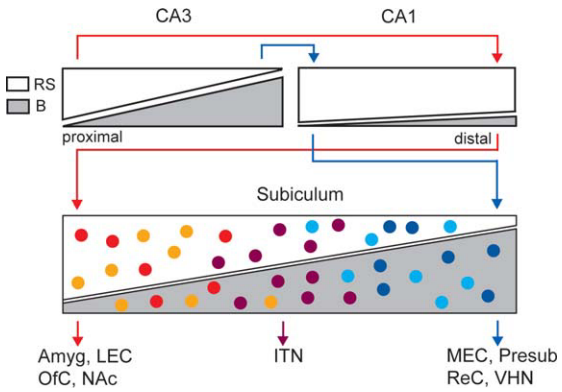

FIGURE 8. Schematic illustration of intrinsic and extrinsic connections in the hippocampal formation and bursting properties of pyramidal neurons. The bursting and regular-spiking neurons are distributed in a gradient along the proximal–distal axis within ca3, ca1, and subiculum. Note that ca1 pyramidal neurons are mostly regular-spiking. The relative distribution of bursting and regular-spiking neurons is shown with gray and white, respectively. Red arrows (top) represent the connections from proximal ca3 to distal ca1 to proximal subiculum, which is mediated primarily by regular-spiking neurons. Blue arrows (top) represent the connections from distal ca3 to proximal ca1 to distal subiculum, which is mediated primarily by bursting neurons. In the subiculum, colored circles indicate neurons projecting to different areas. Subicular subregions along the proximal–distal axis target to distinct sets of brain regions. In each subregion, neurons are intermingled regardless of their projection (red and orange in proximal subiculum, blue, and light blue in distal subiculum). Subicular output (bottom arrows) is composed of a mixture of bursting and regular-spiking cells projecting to each region, with the level of bursting properties determined by the location of the neurons targeting each region. [Color figure can be viewed in the online issue, which is available at wileyonlinelibrary.com.]

firing patterns (Metz et al., 2005; Jarsky et al., 2008; Nowacki et al., in press). Similarly, the distribution of bursting neurons in the subiculum (higher in distal subiculum) is consistent with firing properties recorded from the two subregions in vivo, where higher firing rates were observed in distal subiculum (Sharp and Green, 1994). Given that different regions of subiculum project to different brain areas, the graded distribution of bursting neurons in the subiculum will likely give rise to physiologically distinct effects on the individual target regions.

A variety of effects allow bursting neurons to encode and process information differently than regular spiking neurons (Kepecs and Lisman, 2003). For example, multiple action potentials will elevate presynaptic calcium more than a single action potential, increasing the probability of neurotransmitter release at synapses with otherwise low release probability (Lisman, 1997). Presynaptic bursts can also give rise to increased postsynaptic depolarization by temporal summation (Miles and Wong, 1986; Snider et al., 1998). In addition, bursts of action potentials in the postsynaptic neuron will relieve Mg^{2+} block of NMDA receptors more effectively than single action potentials. Thus, both presynaptic and postsynaptic bursts may enhance calcium entry through NMDA receptors and contribute to increased synaptic plasticity. Consistent with these suggestions, bursting has been shown to be an effective signal for the induction of synaptic plasticity using a variety of protocols (Larson et al., 1986; Huerta and Lisman, 1993; Thomas et al., 1998; Pike et al., 1999; Fortin and Bronzino, 2001; Kampa et al., 2006; Letzkus et al., 2006).

In the subiculum, effects of bursting on synaptic plasticity could result in differences in the activity-dependent modulation of synaptic inputs to the subiculum and outputs from the subiculum to its various targets. In addition, regular-spiking and bursting neurons in the subiculum have been found to exhibit different plasticity rules for both synaptic and nonsynaptic plasticity (Fidzinski et al., 2008; Graves et al., in revision). These inherent differences in plasticity, combined with the different plasticity expected from regular-spiking versus bursting, suggest that plasticity will differ between the two streams of information represented by these two cell types.

Acknowledgments

We thank Drs. William Kath and Il Park for their help in statistic analysis, and Austin Graves and other members of Spruston lab for helpful discussion.

REFERENCES

Amaral DG, Dolorfo C, Alvarez-Royo P. 1991. Organization of CA1 projections to the subiculum: A PHA-L analysis in the rat. Hippocampus 1:415–435.

Brown SP, Hestrin S. 2009a. Cell-type identity: A key to unlocking the function of neocortical circuits. Curr Opin Neurobiol 19:415–421.

Brown SP, Hestrin S. 2009b. Intracortical circuits of pyramidal neurons reflect their long-range axonal targets. Nature 457:1133–1136.

Canteras NS, Swanson LW. 1992. Projections of the ventral subiculum to the amygdala, septum, and hypothalamus: A PHAL anterograde tract-tracing study in the rat. J Comp Neurol 324:180–194.

Cappaert NLM, Wadman WJ, Witter MP. 2007. Spatiotemporal analyses of interactions between entorhinal and CA1 projections to the subiculum in rat brain slices. Hippocampus 17:909–921.

Cooper DC, Moore SJ, Staff NP, Spruston N. 2003. Psychostimulant-induced plasticity of intrinsic neuronal excitability in ventral subiculum. J Neurosci 23:9937–9946.

Donovan MK, Wyss JM. 1983. Evidence for some collateralization between cortical and diencephalic efferent axons of the rat subicular cortex. Brain Res 259:181–192.

Fidzinski P, Shor O, Behr J. 2008. Target-cell-specific bidirectional synaptic plasticity at hippocampal output synapses. Eur J Neurosci 27:1111–1118.

Fortin DA, Bronzino JD. 2001. The effect of interburst intervals on measures of hippocampal LTP in the freely moving adult male rat. Exp Neurol 170:371–374.

Gigg J. 2006. Constraints on hippocampal processing imposed by the connectivity between CA1, subiculum and subicular targets. Behav Brain Res 174:265–271.

Graves AR, Moore SJ, and Spruston N. Differential regulation of intrinsic excitability in distinct cell types of pyramidal neurons of hippocampus. J Neurosci, in revision.

Greene JR, Totterdell S. 1997. Morphology and distribution of electrophysiologically defined classes of pyramidal and nonpyramidal neurons in rat ventral subiculum in vitro. J Comp Neurol 380:395–408.

Groenewegen HJ, Vermeulen-Van der Zee E, te Kortschot A, Witter

MP. 1987. Organization of the projections from the subiculum to the ventral striatum in the rat A study using anterograde transport of *Phaseolus vulgaris* leucoagglutinin. Neuroscience 23:103–120.
Harris E, Witter MP, Weinstein G, Stewart M. 2001. Intrinsic connectivity of the rat subiculum. I. Dendritic morphology and patterns of axonal arborization by pyramidal neurons. J Comp Neurol 435:490–505.
Hirose S, Ino T, Takada M, Kimura J, Akiguchi I, Mizuno N. 1992. Topographic projections from the subiculum to the limbic regions of the medial frontal cortex in the cat. Neurosci Lett 139:61–64.
Huerta PT, Lisman JE. 1993. Heightened synaptic plasticity of hippocampal CA1 neurons during a cholinergically induced rhythmic state. Nature 364:723–725.
Ishizuka N. 2001. Laminar organization of the pyramidal cell layer of the subiculum in the rat. J Comp Neurol 435:89–110.
Ishizuka N, Weber J, Amaral DG. 1990. Organization of intrahippocampal projections originating from CA3 pyramidal cells in the rat. J Comp Neurol 295:580–623.
Jarsky T, Mady R, Kennedy B, Spruston N. 2008. Distribution of bursting neurons in the CA1 region and the subiculum of the rat hippocampus. J Comp Neurol 506:535–547.
Kampa BM, Letzkus JJ, Stuart GJ. 2006. Requirement of dendritic calcium spikes for induction of spike-timing-dependent synaptic plasticity. J Physiol 574:283–290.
Kepecs A, Lisman J. 2003. Information encoding and computation with spikes and bursts. Network 14:103–118.
Kloosterman F, Witter MP, Van Haeften T. 2003. Topographical and laminar organization of subicular projections to the parahippocampal region of the rat. J Comp Neurol 455:156–171.
Larson J, Wong D, Lynch G. 1986. Patterned stimulation at the theta frequency is optimal for the induction of hippocampal long-term potentiation. Brain Res 368:347–350.
Laxmi TR, Bindu PN, Raju TR, Meti BL. 1999. Spatial memory impairment in ventral subicular lesioned rats. Brain Res 816:245–248.
Letzkus JJ, Kampa BM, Stuart GJ. 2006. Learning rules for spike timing-dependent plasticity depend on dendritic synapse location. J Neurosci 26:10420–10429.
Lisman JE. 1997. Bursts as a unit of neural information: Making unreliable synapses reliable. Trends Neurosci 20:38–43.
Mason A. 1993. Electrophysiology and burst-firing of rat subicular pyramidal neurons in vitro: A comparison with area CA1. Brain Res 600:174–178.
Masukawa LM, Benardo LS, Prince DA. 1982. Variations in electrophysiological properties of hippocampal neurons in different subfields. Brain Res 242:341–344.
Mattia D, Hwa GG, Avoli M. 1993. Membrane properties of rat subicular neurons in vitro. J Neurophysiol 70:1244–1248.
Meibach RC, Siegel A. 1977. Efferent connections of the hippocampal formation in the rat. Brain Res 124:197–224.
Menendez de la Prida L, Suarez F, Pozo MA. 2003. Electrophysiological and morphological diversity of neurons from the rat subicular complex in vitro. Hippocampus 13:728–744.
Metz AE, Jarsky T, Martina M, Spruston NR. 2005. R-type calcium channels contribute to afterdepolarization and bursting in hippocampal CA1 pyramidal neurons. J Neurosci 25:5763–5773.
Miles R, Wong RK. 1986. Excitatory synaptic interactions between CA3 neurons in the guinea-pig hippocampus. J Physiol 373:397–418.
Naber PA, Witter MP. 1998. Subicular efferents are organized mostly as parallel projections: A double-labeling, retrograde-tracing study in the rat. J Comp Neurol 393:284–297.
Namura S, Takada M, Kikuchi H, Mizuno N. 1994. Topographical organization of subicular neurons projecting to subcortical regions. Brain Res Bull 35:221–231.
Nowacki J, Osinga HM, Brown JT, Randall AD, Tsaneva-Atanasova K. 2011. A unified model of CA1/3 pyramidal cells: An investigation into excitability. Prog Biophys Mol Biol 105:34–48.
O'Mara S. 2005. The subiculum: What it does, what it might do, and what neuroanatomy has yet to tell us. J Anat 207:271–282.
O'Mara S, Commins S, Anderson M, Gigg J. 2001. The subiculum: A review of form, physiology and function. Prog Neurobiol 64:129–155.
Paxinos G, Watson C. 2007. The Rat Brain in Stereotaxic Coordinates, 6th ed. Academic Press, London.
Pike FG, Meredith RM, Olding AW, Paulsen O. 1999. Rapid report: Postsynaptic bursting is essential for 'Hebbian' induction of associative long-term potentiation at excitatory synapses in rat hippocampus. J Physiol 518:571–576.
Pitkänen A, Pikkarainen M, Nurminen N, Ylinen A. 2000. Reciprocal connections between the amygdala and the hippocampal formation, perirhinal cortex, and postrhinal cortex in rat. A review. Ann NY Acad Sci 911:369–391.
Sharp PE, Green C. 1994. Spatial correlates of firing patterns of single cells in the subiculum of the freely moving rat. J Neurosci 14:2339–2356.
Sneider JT, Chrobak JJ, Quirk MC, Oler JA, Markus EJ. 2006. Differential behavioral state-dependence in the burst properties of CA3 and CA1 neurons. Neuroscience 141:1665–1677.
Snider RK, Kabara JF, Roig BR, Bonds AB. 1998. Burst firing and modulation of functional connectivity in cat striate cortex. J Neurophysiol 80:730.
Sørensen KE. 1980. Ipsilateral projection from the subiculum to the retrosplenial cortex in the guinea pig. J Comp Neurol 193:893–911.
Staff NP, Jung HY, Thiagarajan T, Yao M, Spruston N. 2000. Resting and active properties of pyramidal neurons in subiculum and CA1 of rat hippocampus. J Neurophysiol 84:2398–2408.
Stewart M. 1997. Antidromic and orthodromic responses by subicular neurons in rat brain slices. Brain Res 769:71–85.
Stewart M, Wong RK. 1993. Intrinsic properties and evoked responses of guinea pig subicular neurons in vitro. J Neurophysiol 70:232–245.
Swanson LW, Cowan WM. 1975. Hippocampo-hypothalamic connections: Origin in subicular cortex, not ammon's horn. Science 189:303–304.
Swanson LW, Sawchenko PE, Cowan WM. 1981. Evidence for collateral projections by neurons in Ammon's horn, the dentate gyrus, and the subiculum: A multiple retrograde labeling study in the rat. J Neurosci 1:548–559.
Tamamaki N, Nojyo Y. 1995. Preservation of topography in the connections between the subiculum, field CA1, and the entorhinal cortex in rats. J Comp Neurol 353:379–390.
Taube JS. 1993. Electrophysiological properties of neurons in the rat subiculum in vitro. Exp Brain Res 96:304–318.
Thomas MJ, Watabe AM, Moody TD, Makhinson M, O'Dell TJ. 1998. Postsynaptic complex spike bursting enables the induction of LTP by theta frequency synaptic stimulation. J Neurosci 18: 7118–7126.
Verwer RW, Meijer RJ, Van Uum HF, Witter MP. 1997. Collateral projections from the rat hippocampal formation to the lateral and medial prefrontal cortex. Hippocampus 7:397–402.
Witter MP. 2006. Connections of the subiculum of the rat: Topography in relation to columnar and laminar organization. Behav Brain Res 174:251–264.
Witter MP. 1993. Organization of the entorhinal-hippocampal system: A review of current anatomical data. Hippocampus 3:33–44.
Witter MP, Groenewegen HJ. 1990. The subiculum: Cytoarchitectonically a simple structure, but hodologically complex. Prog Brain Res 83:47–58.
Witter MP, Ostendorf RH, Groenewegen HJ. 1990. Heterogeneity in the dorsal subiculum of the rat. Distinct neuronal zones project to different cortical and subcortical targets. Eur J Neurosci 2: 718–725.
Wyss JM, Van Groen T. 1992. Connections between the retrosplenial cortex and the hippocampal formation in the rat: A review. Hippocampus 2:1–11.